

## Air temperature profile and air/sea temperature difference measurements by infrared and microwave scanning radiometers

D. Cimini,<sup>1,2</sup> J. A. Shaw,<sup>2,3</sup> E. R. Westwater,<sup>4</sup> Y. Han,<sup>4</sup> V. Irisov,<sup>5</sup> V. Leuski,<sup>4</sup> and J. H. Churnside<sup>2</sup>

Received 1 March 2002; revised 5 July 2002; accepted 10 July 2002; published 12 February 2003.

[1] A system of two scanning radiometers has been developed by the National Oceanic and Atmospheric Administration/Environmental Technology Laboratory and deployed on the NOAA R/V *Ronald H. Brown* during the Nauru99 cruise in the tropical western Pacific in June and July 1999. The system is composed of a high-quality temperature sensor and two independent, vertically scanning radiometers, measuring atmospheric and oceanic emission in the microwave (MW), and infrared (IR) regions. Both radiometers measure emission from a uniformly mixed atmospheric gas: oxygen for MW (60 GHz) and carbon dioxide for IR (14.2  $\mu\text{m}$ ). The high atmospheric absorption at these frequencies allows one calibration point from the horizontal atmospheric view using the in situ temperature sensor measurements as a reference. The signal at all other scan angles is scaled relative to that at the horizontal, resulting in a differential technique that is independent of calibration offset. This technique provides continuous and accurate estimates of boundary layer air temperature profile and air/sea temperature difference. The main advantage of this technique is that the water skin temperature can be measured at different optical depths without disturbing the skin layer (magnitude order of microns). We first compare radiometric data collected during the experiment with simulations obtained by atmospheric and oceanic radiative transfer models. We then use statistical inversion techniques to estimate air temperature profiles from upward looking measurements, based on an a priori data set of about 1500 ship-based radiosonde observations. For the “well-posed” problem of air/sea temperature difference estimation, we apply a physical retrieval algorithm to the downward looking measurements, accounting for air attenuation and sea surface roughness. Then we show retrieval results and evaluate the achieved accuracy. Finally, we compare radiometric estimates with in situ measurements, discussing similarities and discrepancies. *INDEX TERMS:* 4504 Oceanography: Physical: Air/sea interactions (0312); 4594 Oceanography: Physical: Instruments and techniques; 3307 Meteorology and Atmospheric Dynamics: Boundary layer processes; 3360 Meteorology and Atmospheric Dynamics: Remote sensing; *KEYWORDS:* air/sea interface, marine boundary layer, scanning radiometers, microwave and infrared radiometry, sea surface temperature

**Citation:** Cimini, D., J. A. Shaw, E. R. Westwater, Y. Han, V. Irisov, V. Leuski, and J. H. Churnside, Air temperature profile and air/sea temperature difference measurements by infrared and microwave scanning radiometers, *Radio Sci.*, 38(3), 8045, doi:10.1029/2002RS002632, 2003.

<sup>1</sup>Centre of Excellence for the Integration of Remote Sensing Techniques and Numerical Modeling for the Forecast of Severe Weather, University of L'Aquila, L'Aquila, Italy.

<sup>2</sup>National Oceanic and Atmospheric Administration/Environmental Technology Laboratory, Boulder, Colorado, USA.

<sup>3</sup>Department of Electrical and Computer Engineering, Montana State University, Bozeman, Montana, USA.

<sup>4</sup>Cooperative Institute for Research in Environmental Sciences, University of Colorado/NOAA Environmental Technology Laboratory, Boulder, Colorado, USA.

<sup>5</sup>Zel Technologies, LLC, Boulder, Colorado, USA.

## 1. Introduction

[2] The interaction between the air and sea plays a dominant role in climate. While above and below the ocean's surface, turbulent mechanisms are responsible for heat and momentum exchanges, the energy fluxes across the air/sea interface are due only to molecular processes [Schuessel *et al.*, 1990]. Marine boundary layer measurements provide important information for this study and many authors have investigated the relationship between the main variables: wind speed, sea surface temperature (SST), atmospheric stability, and sea surface roughness [Smith, 1988; Hwang and Shemdin, 1998; Smirnov, 1994; Pospelov, 1996; Shaw and Churnside, 1997]. Webster and Lukas [1992] recognized that uncertainties in the air/sea temperature difference represent a major uncertainty in assessing energy balance, and encouraged field experiment in the tropical western Pacific (TWP). Fairall *et al.* [1996] showed that to estimate the heat balance to an accuracy of  $10 \text{ W/m}^2$  requires an SST accuracy of  $\pm 0.2 \text{ K}$ .

[3] Monitoring SST with infrared or microwave remote sensors is one of the most useful applications of weather satellites. A common procedure for calibrating or validating satellite data is to compare them with in situ measurements from buoys or ship sensors. This procedure introduces an error because radiometric measurements sense the sea skin layer, whose thickness is less than a millimeter, whereas in situ sensors sound the bulk sea, at a depth of the order of centimeters or even meters [Schuessel *et al.*, 1990]. There is a sensible temperature difference between the skin and the bulk sea, called the interface effect. Other investigators [Fairall *et al.*, 1996; Wick *et al.*, 1996] have expressed the interface effect as a combination of two contributions: the so-called cool skin and warm layer effects. The cool skin regards only the skin layer and is related to the cooling rates by longwave radiation and heat fluxes. It is almost always present, with a contribution of the order of 0.1 to 0.5 K. Conversely, the warm layer is a diurnal phenomenon caused by solar radiation penetrating the upper few meters of the ocean. Depending on solar flux intensity and wind-induced mixing, the warm layer effect ranges between 0 and 3 K, and can eventually mask the net effect of the cool skin [Fairall *et al.*, 1996].

[4] In the last fifteen years, appreciable progress has been achieved in in situ measurements of sea temperature by using drop or floating sondes, but neither technique is capable of measuring the sea skin layer. In fact, in situ sensors can be placed only a few centimeters below the sea surface, and they usually perturb the media by generating mixing and destroying small-scale gradients. The first attempt of using radio-

metric measurements for SST retrievals was by Ewing and McAlister [1960] and McAlister *et al.* [1971] introduced the idea of using two infrared channels with different skin penetration depths to study surface gradients. Trokhimovski *et al.* [1998] pointed out that increasing the penetration depth difference between the two channels would lead to better chances to estimate sea-surface gradients; they also suggested coupling microwave and infrared channels.

[5] In radiometric estimations of SST and air/sea temperature difference we need to account for air absorption and emission and sea surface reflection. Previous field experiments [Bolotnikova *et al.*, 1992; Vesecky *et al.*, 1994] showed that the accuracy of SST retrieval based on microwave measurements at nadir might be 0.5 K or worse. This uncertainty arises primarily from variations in surface emissivity with surface conditions, such as wind speed and foam, whereas a higher accuracy of measuring SST from space-borne infrared sensors can be achieved during cloud free conditions. Moreover, the air/sea temperature difference is estimated by subtracting measurements from air and water sensors and thus, includes two independent errors whose total effect can be of the same order of the estimate. This is true whether the sensors are radiometers or thermometers. Nevertheless, it is possible to achieve a 0.3 K accuracy for microwave SST measurements by using a special radiometer design introduced by Trokhimovski *et al.* [1998]. The idea is to use a radiometer with a single channel at a wavelength with relatively high atmospheric attenuation. Measurements are taken in a vertically scanning mode, sounding radiation at different elevation angles. In a full scanning cycle we sequentially measure natural emission from the atmosphere (upward looking) and from the ocean (downward looking), so we can carefully account for downwelling radiation and sea surface reflection. Assuming the air temperature is constant for horizontal paths shorter than a few hundred meters, the radiation in the horizontal direction can be used as a reference target at the measured air temperature, because of the high local contribution to the emission. Relative measurement of the air and sea skin temperatures is the key to the robustness of this technique. We can apply a differential algorithm that is independent of the radiometer offset, allowing more accurate retrieval of small temperature difference than is possible by subtracting the outputs of two independent sensors. At the same time, this technique can recover air temperature profiles of the boundary layer, providing a relatively simple, yet powerful, tool for marine boundary layer studies. Another technique, which we do not evaluate here, relies on different penetration depths provided by infrared multispectral radiometric measurements [McKeown *et al.*, 1995; Minnett *et al.*, 2001].

[6] Following *Trokhimovski et al.* [1998], other investigators adopted scanning microwave radiometry [*Westwater et al.*, 1998, 1999; *Leusky et al.*, 2000], while *Shaw et al.* [2001] developed and deployed a similar instrument that operated at infrared wavelengths. When using a single remote sensor, retrieval accuracy is difficult to determine because comparisons with bulk measurements are influenced by both cool skin and warm layer phenomena. However, *Trokhimovski et al.* [1998] suggested that this technique results in an air/sea temperature difference retrieval accuracy better than 0.1 K, based on forward model simulations. *Westwater et al.* [1998] found that microwave scanning radiometry yields rms accuracies of the order of 0.4 K for air/sea temperature difference when compared with non-scanning infrared measurements.

[7] In the following, we compare air temperature profile and air/sea temperature difference measurements from two independent scanning radiometers, working at microwave and infrared wavelengths. As anticipated, coupling measurements from the two radiometers could lead to sea surface gradient estimates, but only if the absolute accuracy of each instrument is within 0.1 K [*McAlister et al.*, 1971; *Trokhimovski et al.*, 1998; *Shaw et al.*, 2001]. Experimental data were collected in June and July 1999 during the Nauru99 ship-based experiment, which brought the National Oceanic and Atmospheric Administration's (NOAA) R/V *Ronald H. Brown* (RHB) in the vicinity of Nauru Island (Lat.: 0.521 S, Long.: 166.916 E), in the TWP. In section 2 we describe the instruments and the experimental setup. In section 3 we compare radiometric measurements with theoretical predictions and in section 4 we describe the inversion techniques used for our retrievals. In section 5 we present the results of our estimates, which will be followed by comments and conclusion in section 6.

## 2. Instruments and Experimental Setup

### 2.1. Scanning Radiometry Technique

[8] The principle of the technique is to measure oceanic and atmospheric emission in a wavelength band that exhibits relatively high atmospheric attenuation. In this case, the radiation in the horizontal direction can be used as a reference level since the brightness temperature is essentially equal to the air temperature at the measurement height; thus, an accurate air temperature measurement would provide a calibration of the radiometer offset. This calibration technique is as precise as the air temperature sensor reading when the atmosphere is uniform over a horizontal distance of the order of radiometer's atmospheric optical depth (150 to 300 m). The band must provide

enough atmospheric absorption to yield an accurate local air temperature measurement in the horizontal scan direction, while being low enough that the radiometer can still see the sea-surface emission from the deployment height. From the upward looking scan we can retrieve atmospheric air temperature gradients with respect to surface air temperature. Adding the high-quality temperature sensor measurements, we obtain the air temperature profile up to 500 m.

[9] Relative measurement of air and water skin temperatures is the key to the robustness of the scanning technique. Calibration does not depend on the absolute accuracy because we retrieve the temperature difference only from the corresponding radiometer voltage changes between horizontal and downward views. The resulting temperature difference is independent of the radiometer offset and allows more robust retrieval of small temperature differences than is possible when subtracting the outputs of two independent sensors.

### 2.2. Instrumentation

[10] Our system is composed of two vertically scanning radiometers (SR), one operating in the microwave (MW) and the other in the infrared (IR) spectral region, and a high-quality air temperature sensor (Vaisala HMP 233 Met sensor). A picture of the deployment is shown in Figure 1. Each radiometer measures natural emission in the proximity of a uniformly mixed atmospheric gas absorption band, oxygen for the MWSR, and carbon dioxide for the IRSR. Both radiometers are designed for precise and continuous estimation of air/sea temperature difference and for recovery of air temperature profiles (height from 0 to 500 m). Each radiometer beam scans continuously in a vertical plane using an independent rotating mirror, so that the radiometers measure air and sea brightness temperature at different angles. By using such a circular scanning mode, the sky and ocean brightness temperatures were sequentially measured. The infrared wavelength region was selected to have atmospheric weighting functions closely approximating those of the MWSR. In this case, the atmospheric scans of the instruments should yield similar angular emission spectra, but the emission from the ocean surface is different at MW and IR wavelengths. A summary of the radiometers' main characteristics is shown in Table 1. Notice that the IRSR water penetration depth is approximately two orders of magnitude smaller than that of the MWSR. According to theoretical computations [*Trokhimovski et al.*, 1998] the difference between the sea surface temperature measurements from the two radiometers can be up to 0.4 K.

[11] The MWSR was built by the Lebedev Physical Institute of the Russian Academy of Sciences in Moscow, Russia. This device was first used on a research

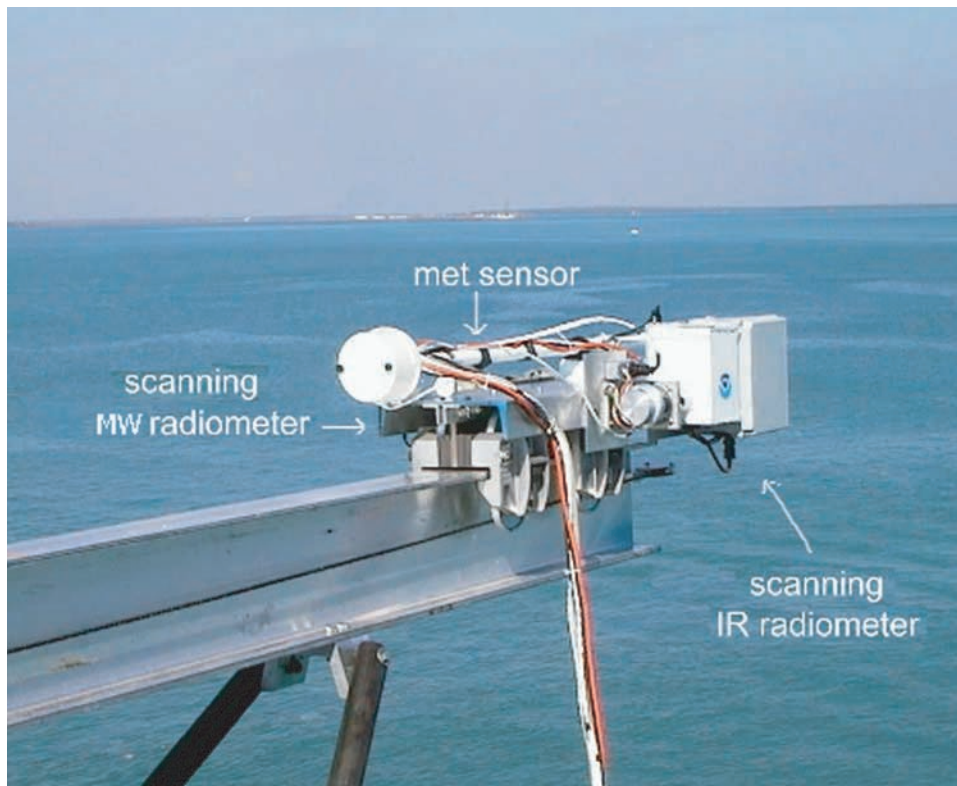


**Figure 1.** Picture of the scanning radiometer system.

vessel during the Joint US-Russia Internal Waves Experiment (JUSREX) in July 1992 [Trokhimovski *et al.*, 1998]. The MWSR consists of a total power compensation-type radiometer, which operates near the peak of the oxygen absorption band at 60 GHz, with a bandwidth of about 4 GHz. The antenna has a main beam width of  $6.6^\circ$  at the 3 dB level and receives vertical polarization. Because the mirror reflects, the polarization plane rotates during the scan. Near nadir, the water surface is observed at horizontal polarization while at grazing angles at vertical polarization. At this frequency, the water penetration depth is estimated to be about 0.3 mm, while the atmospheric optical depth is about 300 m. The radiometer sensitivity was found to be about 0.02 K at an integration time of 1 s. The instrument's details are fully described by Trokhimovski *et al.* [1998].

[12] The IRSR was designed and built at NOAA/ETL [Shaw *et al.*, 2001] and it was first deployed during this experiment. It operates with a single wavelength channel that is centered on  $14.2 \mu\text{m}$ , on the short-wavelength edge of a carbon dioxide absorption band, with a  $1.1 \mu\text{m}$  bandwidth. Changes in the horizontal radiance indicate local air temperature changes at the instrument height, as long as we avoid operating in the vicinity of a carbon

dioxide source (such as engine exhaust). The system optics result in a  $0.9^\circ$  full-angle field of view. As shown in Figure 2, a bandpass interference filter behind the lens provides a spectral bandwidth centered at  $14.20 \mu\text{m}$  with half-power points at  $13.63 \mu\text{m}$  and  $14.76 \mu\text{m}$ . The zenith downwelling atmospheric radiance spectrum matches a blackbody curve at the local air temperature near the center of the carbon dioxide absorption band at  $668 \text{ cm}^{-1}$  ( $14.97 \mu\text{m}$ ), and remains highly opaque up to about  $700 \text{ cm}^{-1}$  ( $14.3 \mu\text{m}$ ). Thus, the long-wave end of the filter bandwidth sees primarily the air immediately in front of the radiometer, and the short-wave end provides

**Table 1.** Characteristics of the Scanning Radiometers

	MWSR	IRSR
Central line	60 GHz	$14.2 \mu\text{m}$
Band width	4 GHz	$1.1 \mu\text{m}$
Beam width	$6.6^\circ$	$1^\circ$
Scanning rate	0.55 Hz	0.55 Hz
Main emitter	oxygen	carbon dioxide
Sea emissivity	0.45	0.98
Optical depth	300 m	150 m
Penetration depth	$300 \mu\text{m}$	$3 \mu\text{m}$
Polarization	V	negligible

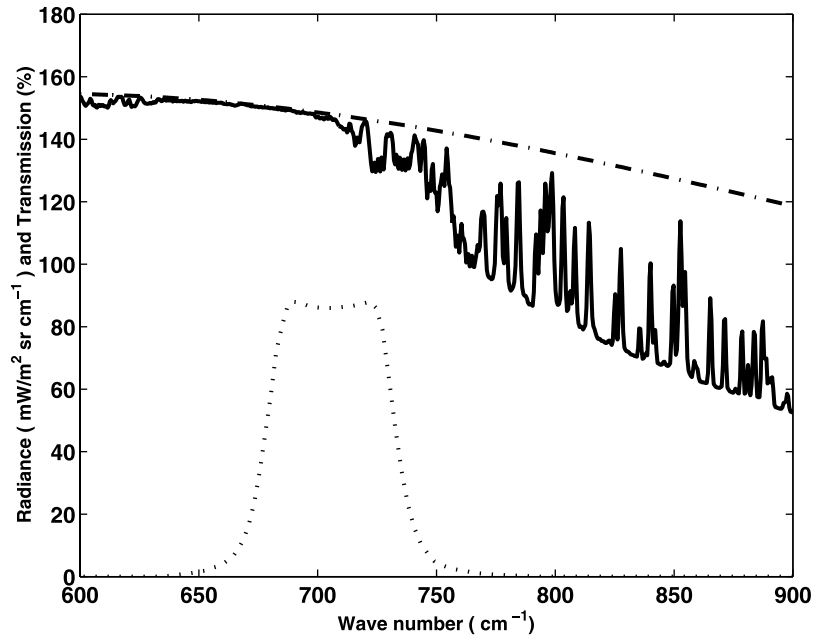


**Figure 2.** Spectrum of IRSR filter function (dotted line), atmospheric emission at zenith measured by FTIR (solid line), and the Planck function evaluated at ambient temperature (dash-dotted line).

most of the scan-angle-dependent radiance. The band-average atmospheric optical depth, weighted by the filter bandwidth, is 150 m. The water penetration depth for this infrared bandwidth is only  $3 \mu\text{m}$ .

### 2.3. Calibration

[13] During the Nauru99 experiment we were not able to use the usual calibration approach of viewing two high-quality blackbody sources because the radiometers were operating from a boom extended out over the ocean, with the computer and associated electronics housed in a protective trailer on the deck of the ship. Even in calm seas, a blackbody surface could be ruined in a short period of time by sea salt. Nevertheless, for future deployments, we intend to modify the scanning radiometer system to include at least one integral source, which would provide, together with the horizontal view, the two needed calibration targets.

[14] However, MWSR gain calibration was based on laboratory tests and comparison with simulated scans obtained from radiosonde temperature profile data and the Rosenkranz 98 Radiative Transfer Model (RTM) [Trokhimovski *et al.*, 1998; Rosenkranz, 1998]. We also apply a correction depending on the radiometer's internal temperature. Radiometer offset was continuously determined during measurements by using the emission from the horizontal direction as a calibration point, since the brightness temperature is essentially equal to the air

temperature at the measurement height. However, all analyses were based on the difference between brightness temperatures at various angles and at horizontal viewing; thus, absolute values of brightness temperature were not required for the computation.

[15] Prior to deployment, we measured the IRSR gain for several hours by continuously scanning across two blackbody calibration sources. We found that the gain drifted slowly enough that an adjustment once every several hours provides sufficient calibration. During deployment, one reference calibration point was provided during each scan by relating the horizontally viewing radiometer voltage to the local measured air temperature. For the second calibration point we used measurements from a Fourier Transform InfraRed (FTIR) spectroradiometer that was deployed on the same ship for high-accuracy measurements of atmospheric emission spectra. We averaged the atmospheric emission spectra measured by the FTIR over the optical bandwidth of the IRSR to derive an equivalent radiance for the vertical radiometer view, and we averaged the Planck function, evaluated at the local air temperature, over the radiometer bandwidth to derive an equivalent radiance for the horizontal radiometer view (Figure 2). We calibrated in terms of radiance, with which the radiometer signal varies linearly, but then computed an equivalent brightness temperature gain so that we could express some results in the more physically intuitive units of temperature.

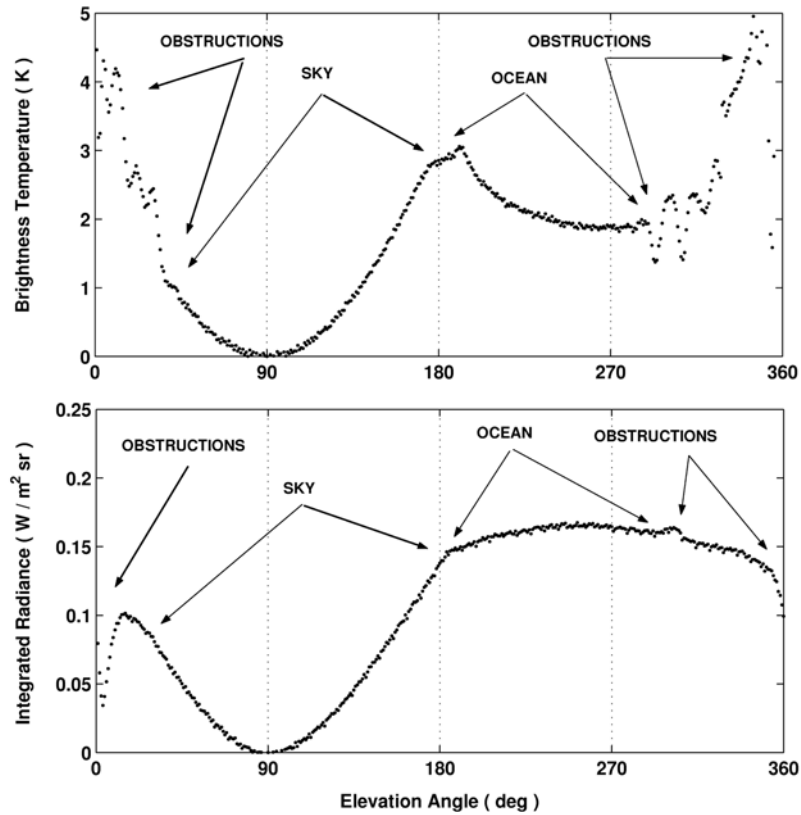


**Figure 3.** Typical scan for the MWSR (top) and IRSR (bottom), with data averaged for 30 min. Vertical axes units are relative to the zenith view.

[16] Using the FTIR spectra to calibrate the scanning radiometer zenith data required identifying clear versus cloudy periods. The short-wavelength end of the scanning radiometer filter response allows the IR scanning radiometer to see higher into the atmosphere than desired, resulting in zenith-signal variations when low clouds pass overhead. We were able to identify cloudy periods from the temporal variability of FTIR data and from a laser ceilometer operated by NOAA/ETL aboard the same ship. Because of the high accuracy achievable by the FTIR, the IRSR overall calibration uncertainty is estimated to be better than 0.2 K [Shaw *et al.*, 2001].

#### 2.4. System Deployment

[17] The two scanning radiometers, together with the Vaisala HMP 233 temperature and humidity sensor, were mounted on a trolley, able to move back and forth along a boom mounted on the roof of a mobile laboratory built from a standard sea container. The boom extended 5 m beyond the port side of the R/V RHB, at a height of 10 m ASL (Figure 1). The trolley enabled the entire radiometer package to be brought onto the roof of the sea container

where an operator could fill the liquid-nitrogen dewar, clean the mirrors, or run a full radiometer calibration with the temperature probe and an auxiliary blackbody source. The boom-and-trolley configuration kept the scanning radiometers above the water, and allowed easy and convenient access to the instruments when needed. During periods of transit through heavy seas, the radiometers were locked in position on the sea-container roof and covered. The optics were well protected throughout the experiment; only the scanning mirrors required cleaning but no more than once daily.

#### 2.5. Scanning Procedure

[18] With the current system, a variable scan rate was set at the same frequency (0.55 Hz) for both the mirrors, corresponding to one scan every 1.8 s. No additional modulation except the antenna beam rotation was applied to the radiometers. A typical pair of measured scans, averaged for 30 min, is shown in Figure 3, after angle and relative voltage-to-kelvin calibrations. The mirrors were scanning in opposite direction: looking from the ship, the IRSR scan mirror rotated clockwise

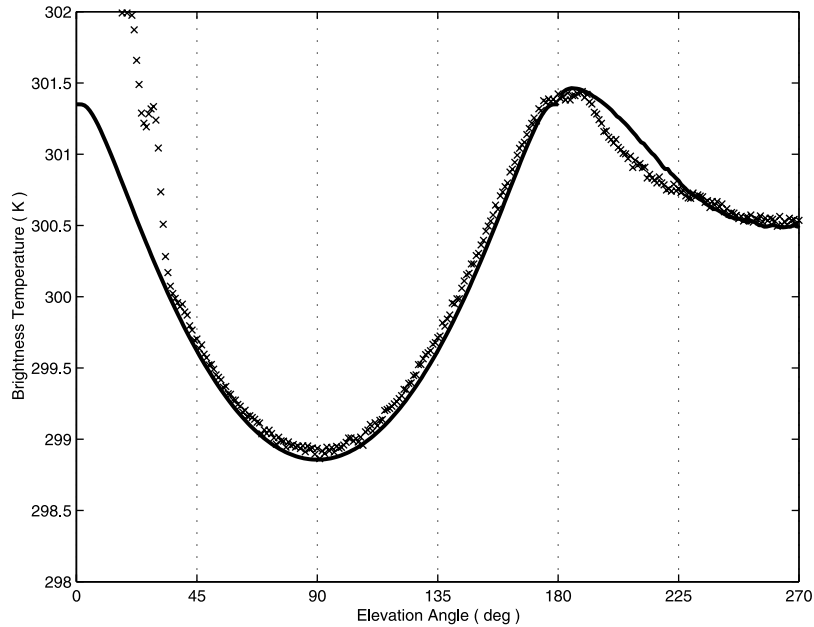


**Figure 4.** Comparison of measured (crosses) and modeled (solid line) upward and downward looking MWSR scans. The model is based on a radiosonde launched at 05:24, 07/05/1999 UTC, and the radiometric measurements are from 05:15 to 05:45 UTC. The air/sea difference value was set to  $-0.31$  K, which was the retrieved value at this time.

while the MWSR mirror scanned counterclockwise. The typical scanning sequence is: for elevation angles from  $0^\circ$  to  $40^\circ$ , both radiometers have a view obstructed by the boom on which they are mounted; between  $40^\circ$  and  $180^\circ$  (horizon), the radiometers look up at the sky, showing symmetrical measurements with respect to  $90^\circ$  (zenith); past the horizon, both radiometers look down at the ocean, reaching nadir position at  $270^\circ$ ; from  $280^\circ$  to  $360^\circ$ , the boom again enters the radiometer beams, leaving about  $240^\circ$  of unobstructed view.

[19] Figure 3 shows that the antenna beam widths are different, which leads to different obstructed portions of the total scan. Analyses presented in the following sections were made by using data with 10 min averaging. For such an averaging time, the radiometer's noise contributes negligibly to errors of air and water temperature determination. During this 10-min averaging time, care was taken to avoid cloudy conditions.

### 3. Forward Problem

[20] Before introducing the inversion techniques, it is worth studying the direct problem. Such an approach compares radiometric measurements with theoretical predictions from a RTM based on fundamental physics [Clough *et al.*, 1992; Liebe and Layton, 1987]. Supplying the model with radiosonde-measured profiles of

meteorological variables such as pressure, temperature, and water vapor density, we calculate the spectral and/or angular distribution of radiance [Westwater, 1993]. Then we compare simulated measurements with simultaneous observation from the MWSR and IRSR. If the observations and calculations agree to within the uncertainty of the radiometer measurements, confidence is obtained in the instrument data. However, if measurements that are believed to be accurate agree poorly with calculations, this comparison can lead to improvements in the forward models parameterization [Han *et al.*, 1997].

[21] In the following section we explain the theoretical background and the results of solving the direct problem both for upward and downward looking infrared and microwave radiation.

#### 3.1. Modeling Upward Looking Scan

[22] To solve the direct problem in the infrared region of the spectra, we used both the Line-by-Line Radiative Transfer Model (LBLRTM) [Clough *et al.*, 1992; Clough, 1995] and the Moderate Resolution Radiative Transfer Model MODTRAN4 [Bernstein *et al.*, 1996; Berk *et al.*, 1998]. On extensive computations on a priori data sets, we used only MODTRAN4, because of greatly reduced computer time. We computed infrared spectra between  $600\text{ cm}^{-1}$  and  $1000\text{ cm}^{-1}$  for different slant paths, changing the simulation elevation angle from horizon to

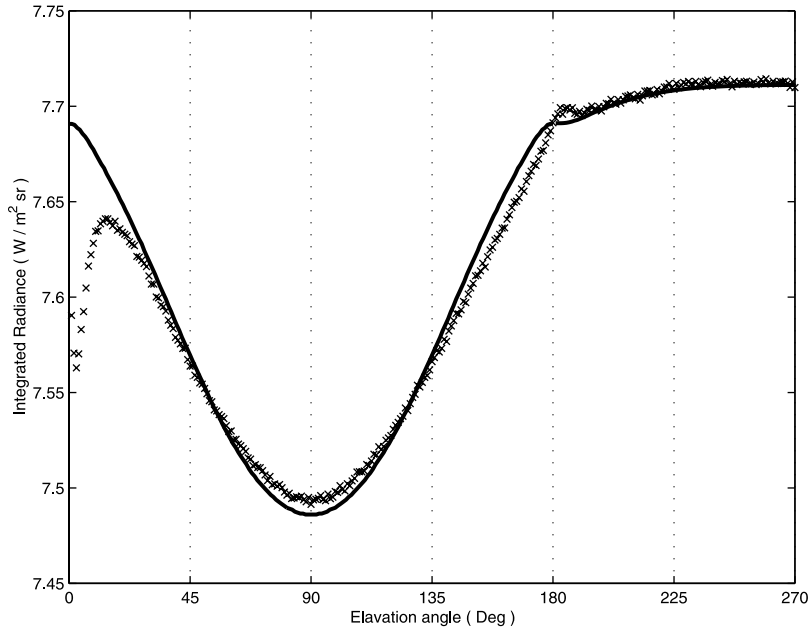


**Figure 5.** Comparison of measured (crosses) and modeled (solid line) upward and downward looking IRSR scans. The RAOB was launched at 05:24, 07/05/1999 UTC; the radiometric measurements are from 05:15 to 05:45 UTC. The air/sea difference value was set to  $-0.39$  K, which is the retrieved value at this time.

zenith. Then, we simulated the IRSR measurement scans by convolving the IRSR filter function (Figure 2) with the computed spectrum at each scanning angle.

[23] To simulate MWSR measurements, we used the NOAA/ETL RTM [Schroeder and Westwater, 1991] with the Rosenkranz 98 absorption model. Thus we computed downwelling brightness temperatures at the MWSR central frequency (60 GHz) for ninety angles from horizon to zenith.

[24] In Figure 4 are shown typical measured and simulated MWSR scans. The upward looking part corresponds to elevation angles from  $0^\circ$  to  $180^\circ$  (zenith is at  $90^\circ$ ). For those angles where the radiometer beam was not obstructed, the residual between the two remains within the total estimated accuracy. Figure 5 shows the equivalent of Figure 4, but for IRSR measured and simulated scans; again, we can see that the difference remains within the total estimated accuracy. To account for antenna smoothing, we averaged over angles by assuming a Gaussian beam.

### 3.2. Modeling Downward Looking Scans

[25] During half of each scan, both scanning radiometers were measuring upwelling radiation, looking down in all the directions between the angles of  $-90$  and  $+90^\circ$  with respect to nadir. Although the upward looking scan looks similar for both the instruments, this

is not the case for the downward looking scan, because the water dielectric constant ( $\delta$ ), emissivity ( $\epsilon$ ) and reflectivity ( $\rho$ ) differ in the microwave and infrared regions of the spectrum. According to theory, we have a nadir sea-surface emissivity of about 0.45 at the MWSR operation frequency, while it is greater than 0.98 in the IRSR band. Another important difference between the two radiometers is that IRSR optics depends negligibly on polarization direction, whereas the MWSR is strongly polarization dependent.

[26] We also have to consider that the sea surface is not a flat Fresnel surface, but is roughened by the whole surface-wave spectra, ranging from tidal to capillary waves. If the wavelength of radiation is small compared to the surface curvature, it can be assumed that the scattered field at each point on the surface is equivalent to that resulting from a plane tangent to the surface at that point. That is definitely true in the infrared region, but also acceptable in the microwave. We also assume that the radiometer beam at the sea surface is large enough to cover a statistically significant amount of single capillary waves. In this case, we can model the sea-surface total emission and reflection as the integral of the contributions from a two-dimensional probability distribution of wave slopes. We use the Shaw-Churnside [Shaw and Churnside, 1997] mean square slope for the distribution of ocean waves. This theory represents a validation and an improvement of the Cox-Munk [Cox

and Munk, 1954] results, introducing a correction depending on atmospheric stability. In modeling the sea rough surface emissivity and reflectivity we account for geometrical effects, such as wave shadowing or surface-emitted-surface-reflected radiation. Even so, the results might be inaccurate for nadir angle greater than  $75^\circ$ , where such effects are dominant and the path from the sea surface to the instrument is much longer [Mikhailova and Fuks, 1993; Wu and Smith, 1997; Nalli et al., 2001]. The relative correction induced by sea surface roughness is larger for the MWSR than for the IRSR, but in both cases the normalized contrast (i.e., the difference between upwelling radiation computed with a plane sea surface and a rough sea surface, divided by the total range of variability during the scan) is of the order of few percent. The upwelling radiation reaching the radiometer antenna is a combination of three contributions. The first is the thermal emission from the sea, the second is the downwelling radiation reflected by the sea surface while the third is the thermal emission from the air layer in between the radiometer and the sea surface. In the microwave region, we can express the upwelling radiation in terms of brightness temperature ( $Tb$ ) as [Trokhimovskii et al., 1998]:

$$Tb_{Plane}^\uparrow(\vartheta) = Tb^\downarrow(\vartheta)\rho(\vartheta)e^{-2\tau} + T_{Sea}(1 - \rho(\vartheta))e^{-\tau} + T_{Air}(\rho(\vartheta)e^{-\tau} + 1)(1 - e^{-\tau}). \quad (1)$$

Here we introduce  $\vartheta$  as the incidence angle and  $\rho(\vartheta) = \rho_V(\vartheta)\sin^2\vartheta + \rho_H(\vartheta)\cos^2\vartheta$  is the sea surface reflectivity factor that accounts for MWSR waveguide polarization, which is rotated by the scanning mirror. This equation is valid in the Fresnel surface approximation, but when considering sea surface roughness it becomes:

$$Tb_{Rough}^\uparrow(\vartheta) = \int_{\varphi_x} \int_{\varphi_y} P(\varphi_x, \varphi_y) \cdot Tb_{Plane}^\uparrow(\vartheta) d\varphi_x d\varphi_y, \quad (2)$$

where  $P(\varphi_x, \varphi_y)$  is the two-dimensional sea slope distribution, and  $\varphi_x$  and  $\varphi_y$  are the slope angles between the horizontal plane and the sea surface. In the infrared region we express upwelling radiation in terms of radiance integrated over the IRSR filter function. In the Fresnel approximation we have:

$$\overline{L_{Plane}^\uparrow(\vartheta)} = \overline{L^\downarrow(\vartheta)}\rho(\vartheta)e^{-2\tau} + \overline{B(T_{Sea})}(1 - \rho(\vartheta))e^{-\tau} + \overline{B(T_{Air})}(\rho(\vartheta)e^{-\tau} + 1)(1 - e^{-\tau}); \quad (3)$$

while considering sea surface roughness, it becomes:

$$L_{Rough}^\uparrow(\vartheta) = \int_{\varphi_x} \int_{\varphi_y} P(\varphi_x, \varphi_y) \cdot L_{Plane}^\uparrow(\vartheta) d\varphi_x d\varphi_y. \quad (4)$$

In equations (1) and (3),  $\tau(\vartheta) = \int_0^d \alpha(T_{Air}) dz \approx \overline{\alpha(T_{Air})} \cdot d = \overline{\alpha(T_{Air})} \cdot h / \cos(\pi - \vartheta)$  is the band-averaged optical thickness ( $\alpha$  is the atmospheric absorption coefficient at temperature  $T_{Air}$ ,  $d$  is the effective path length, and  $h$  is the height of the sensor), while  $B(T_{Sea})$  and  $B(T_{Air})$  represent the Planck function spectra evaluated respectively at the sea and air temperatures. In equations (3) and (4), we use  $\overline{L}(\vartheta)$  to represent band-averaged radiance. Implicit are the assumptions that air temperature is constant in the layer below the radiometers and that  $\tau$  does not change significantly over the band from its spectral average over the IRSR filter function.

[27] In Figure 4, for elevation angles between  $180^\circ$  and  $270^\circ$ , we show MWSR downward looking measurements and the corresponding modeled scan. Except within the region from  $200$  to  $220^\circ$ , the agreement is better than  $0.1$  K. In general, scattering models have poorer accuracy for larger nadir angles, and, in addition, there is more uncertainty due to large field of view. The downward looking measured and modeled IRSR scans are shown in Figure 5, for elevation angles ranging from  $180$  to  $270^\circ$ . As for the MWSR, the largest discrepancies appear at grazing angle (elevation angle  $180$ – $190^\circ$ ), but the overall agreement looks promising. Note that grazing angle measurements are not used in the retrieval, neither for the MWSR nor for the IRSR.

## 4. Retrieval Technique

[28] The MW and IR scanning radiometers are both designed for precise and continuous estimation of air/sea temperature difference and for recovery of air temperature profiles up to  $500$  m. We collected MWSR and IRSR measurements with the same time stamp, but we calibrated and processed them independently, obtaining two completely independent retrievals. In this section we describe the retrieval techniques we applied to MWSR and IRSR measurements to solve the inverse problems.

### 4.1. Air Temperature Profile

[29] Atmospheric radiation observations from the upward looking scan were used to estimate air temperature profiles by using a variation of linear statistical inversion described by Westwater [1993]. An a priori set of contemporary profiles and ground-based radiometric measurements was required.

[30] We first collected a set of about fifteen hundred ship-based radiosonde observations (RAOBs), launched during the 1992 to 1993 tropical ocean global atmosphere coupled ocean-atmosphere response experiment (TOGA-COARE) [Webster and Lukas, 1992] from eight research vessels sailing in the tropical Pacific Ocean. For each of the RAOBs we computed two simulated measurement scans, one corresponding to the MWSR and one to the IRSR. In the MW region, we used RTM routines

with the Rosenkranz 98 absorption model [Rosenkranz, 1998] to compute atmospheric brightness temperature at the MWSR central frequency as a function of the elevation angle. For the IRSR we ran MODTRAN4 [Bernstein *et al.*, 1996; Berk *et al.*, 1998] to generate the atmospheric emission spectrum between  $600 \text{ cm}^{-1}$  and  $1000 \text{ cm}^{-1}$  for each elevation angle, and then we integrated over the filter function. Thus we obtained an a priori data set composed of 1455 atmospheric temperature profiles and simultaneous MWSR and IRSR simulated measurements.

[31] We next performed empirical orthogonal function (EOF) decomposition [Strang, 1980] to determine the most significant basis functions representing the a priori data set. This technique is widely used because it reduces computation resources and enhances inversion stability. We found that to capture variations above the instrumental noise level of 0.2 K, only three EOFs were required for the MWSR and four for the IRSR. Projection of the measured radiation on the EOFs and the subsequent application of linear statistical inversion resulted in temperature profile estimates.

[32] From the prepared a priori data set we are also able to predict the retrieval error expected for each of the instruments. With this technique, air temperature profile retrieval accuracy is estimated to be better than 0.4 K rms up to 500 m for the IRSR and better than 0.3 K for MWSR. The vertical resolution for the retrieved profiles ranges from about 10 m near the surface to about 300 m at 500 m altitude [Westwater *et al.*, 2000].

## 4.2. Air/Sea Temperature Difference

[33] For air/sea temperature retrieval we used a different approach, based on a physical, rather than statistical, inversion method. This is appropriate because, in contrast to the air temperature profile retrieval, the air/sea temperature retrieval is a “well-posed” problem. The definition of well-posed problem has been introduced by Hadamard [1932]. A problem is well-posed if it meets three conditions: (1) for each element of the input space exists a solution; (2) this solution is unique; (3) the solution is stable. Starting from the direct problem, expressed by (2) and (4), we solved it analytically to get a solution for  $\Delta T_{SA} = T_{Sea} - T_{Air}$ .

[34] Theoretically, given the complete angular set of downwelling radiation, a measurement from a single downward looking angle would provide an air/sea temperature estimate, but, to reduce errors induced by inhomogeneity, we average the retrieval results from about ten angles. We used elevation angles between  $220^\circ$  and  $230^\circ$  ( $45 \pm 5^\circ$  off nadir) as a trade-off between large nadir angles (for which the sea surface model may be inaccurate) and small nadir angles (where there might be a small residual effect from the boom). The retrieval robustness was tested for different perturbation sources. We inde-

pendently checked output changes from an input perturbation of 1 K on air temperature, or  $1^\circ$  in zenith position or 5 psu on sea salinity, and in all cases found a retrieval difference of the order of hundredths of a Kelvin.

[35] For radiometric data measured from MWSR we used a similar approach described by Trokhimovski *et al.* [1998]. Introducing into (2) the relative brightness temperatures  $\Delta Tb^\uparrow = Tb^\uparrow - T_{Air}$  and  $\Delta Tb^\downarrow = Tb^\downarrow - T_{Air}$ , the local incident ( $\vartheta_l$ ) and the zenith reflection ( $\vartheta_r$ ) angles, we can solve for  $\Delta T_{SA} = T_{Sea} - T_{Air}$ :

$$\Delta T_{SA} = T_{Sea} - T_{Air} = \frac{\Delta Tb^\uparrow(\vartheta) - \iint P(\varphi_x, \varphi_y) \Delta Tb^\downarrow(\vartheta_r) \rho(\vartheta_l) e^{-2\tau(\vartheta)} d\varphi_x d\varphi_y}{\left(1 - \iint P(\varphi_x, \varphi_y) \rho(\vartheta_l) d\varphi_x d\varphi_y\right) e^{-\tau(\vartheta)}}. \quad (5)$$

As already mentioned, this physical inversion method is independent of absolute accuracy of air temperature measurement. In the IR region we solved the radiative transfer equation (4), with the assumptions we introduced before, to obtain the integrated blackbody radiance emitted by the sea surface  $\overline{B(T_{Sea})}_\vartheta$  at the observation angle [McKeown *et al.*, 1995]:

$$\overline{B(T_{Sea})}_\vartheta = \frac{L_{Tot}^\uparrow(\vartheta) - \rho(\vartheta_l) \cdot e^{-2\tau(\vartheta)} L_{Tot}^\downarrow(\vartheta_r) - \rho(\vartheta_l) \cdot e^{-\tau(\vartheta)} (1 - e^{-\tau(\vartheta)}) B(T_{Air}) - (1 - e^{-\tau(\vartheta)}) B(T_{Air})}{(1 - \rho(\vartheta_l)) \cdot e^{-\tau(\vartheta)}}, \quad (6)$$

which leads to:

$$\Delta T_{SA} \propto B(T_{Sea}) - B(T_{Air}) = \frac{\Delta L_{Tot}^\uparrow(\vartheta) - \iint P(\varphi_x, \varphi_y) \Delta L_{Tot}^\downarrow(\vartheta_r) \rho(\vartheta_l) e^{-2\tau(\vartheta)} d\varphi_x d\varphi_y}{\left(1 - \iint P(\varphi_x, \varphi_y) \rho(\vartheta_l) d\varphi_x d\varphi_y\right) e^{-\tau(\vartheta)}}. \quad (7)$$

In (6) and (7),  $L_{Tot}^\uparrow(\vartheta)$  and  $L_{Tot}^\downarrow(\vartheta)$  refer to upwelling and downwelling radiance. Once we obtain  $\overline{B(T_{Sea})}_\vartheta$ , we compute the difference between this quantity and the integral of the Planck blackbody function at temperature  $T^*$ . The estimated sea temperature is finally computed as the value that minimizes this difference over the set of observation angles.

## 5. Results

[36] In this section we present results obtained by applying the techniques described in section 4 to MWSR and IRSR measurements, to retrieve air temperature profiles and air/sea temperature differences.

### 5.1. Air Temperature Profiles

[37] Figure 6a shows an example of air temperature profiles measured by a balloon and retrieved from

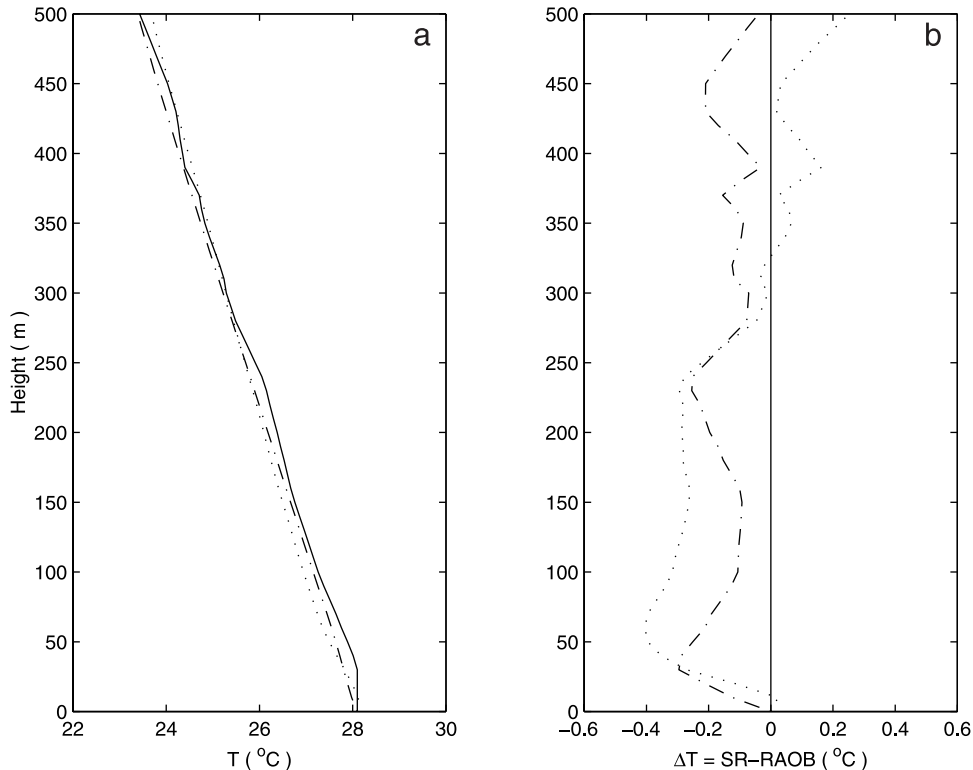
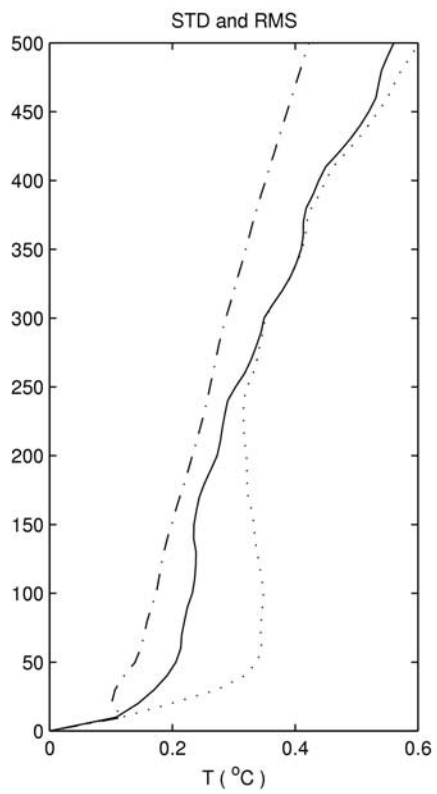
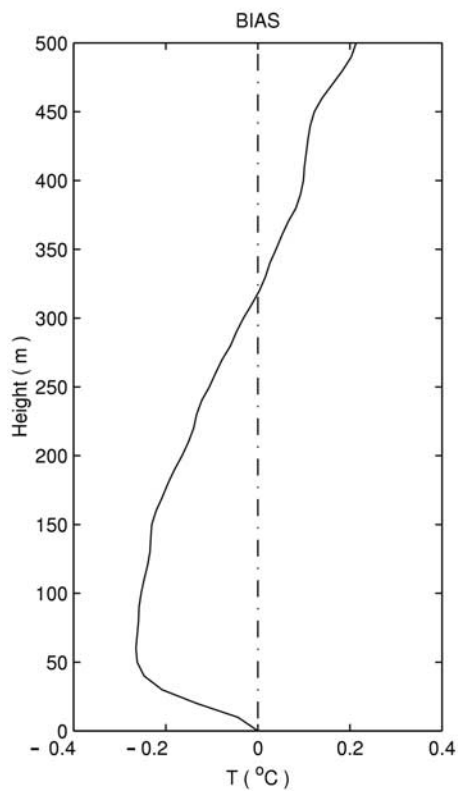
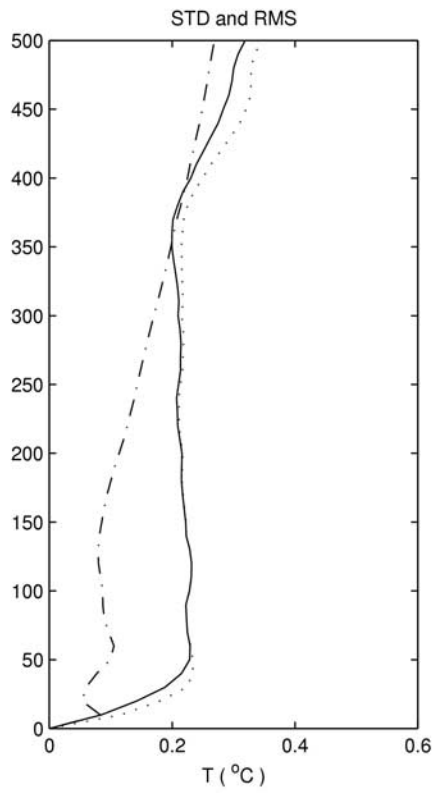
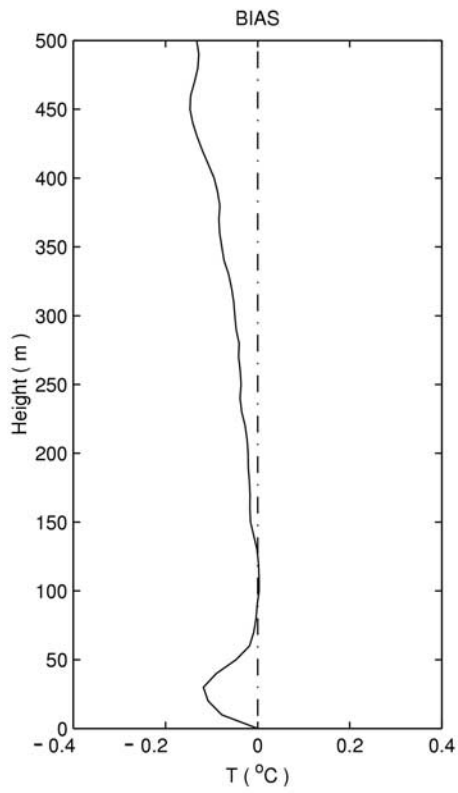


**Figure 6.** (a) Air temperature profile in situ measurements (solid line) and radiometric retrievals. The RAOB was launched at 23:25, 07/03/1999 UTC, while radiometric data were taken between 23:20 and 23:50 UTC. (b) Difference between in situ measurements and radiometric estimates (dotted: IRSR, dash-dotted: MWSR).

MWSR and IRSR upward looking measurements. We averaged the retrieved temperature profiles that fell within  $\pm 15$  min from the RAOB starting time. In Figure 6b we show the difference between in situ and remote measurements, which in this case does not exceed 0.4 K for altitudes lower than 500 m. Considering the whole set of RAOBs launched from R/V RHB between 1999/07/03 and 1999/07/07, we can compute statistics of the overall comparison. In Figure 7 we plotted the mean value (BIAS), standard deviation (STD), and the root mean square (RMS) difference between radiometric estimates and in situ measurements for the whole sample. For the MWSR (top) the STD remains lower than 0.3 K up to 500 m, while the RMS exceeds that value only for levels higher than 450 m. The BIAS does not exceed 0.16 K, but shows an unexpected peak around 30 m. It is useful to remember that RAOB measurements in the lowest tens of meters are sometimes questionable, being influenced by the ship environment in which they are launched. Besides this, the MWSR shows an air temperature profile retrieval accuracy comparable with the

predicted error, estimated from the prepared a priori data set. The IRSR (bottom) shows a STD profile that increases with height, reaching almost 0.6 at 500 m, which is consistent with the prediction from the a priori data set. On the other hand it is affected by a fairly high BIAS (up to 0.3 K), which increases the RMS between 30 m and 250 m. This might be related to the relatively small sample (22 cases), but also to the calibration procedures, which relies on FTIR atmospheric emission spectra measurements.

[38] A powerful feature of radiometrically derived air temperature profiles is the high temporal resolution achievable. During Nauru99 balloons were launched from 4 to 8 times per day, while scanning radiometers were working continuously, at a rate of one scan every 1.8 s. Averaging was needed to reduce internal noise and external high-frequency variations, but the instrument sensitivity permits an accurate retrieval with just 3 min averaging. Figure 8 shows an 18-daytime series of air temperature retrieved from 10 min averaged MWSR scans. The diurnal heating cycle is clearly shown (Nauru



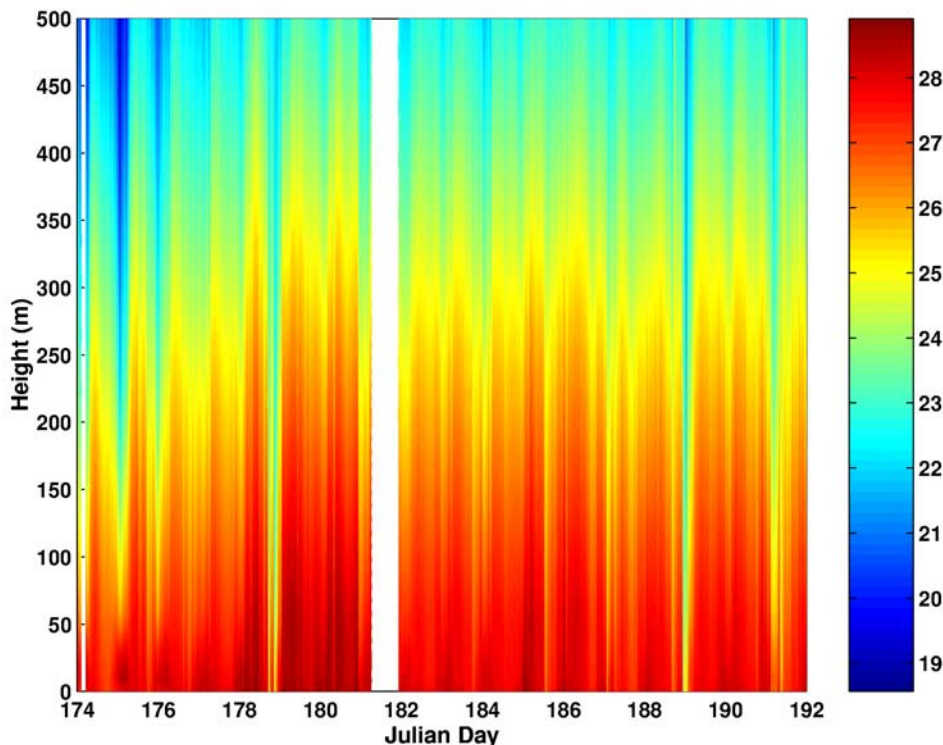


**Figure 8.** Eighteen-day time height cross sections of air temperature profiles retrieved from 10 min averaged MWSR upward looking scans. Julian day 174 is 1999/06/23 while 192 is 1999/07/11 UTC. The temperature color scale is in units of  $^{\circ}\text{C}$ .

noon = 2400 UTC); also, cooling events around Julian days 179, 189, and 191.5 were associated with rain.

## 5.2. Air/Sea Temperature Differences

[39] In Figure 9 we show a five-day time series of air/sea temperature difference retrieved from downward looking MWSR and IRSR scans as well as from bulk measurements. Estimates were obtained by averaging measured scans for 10 min to reduce instrumental random noise, short-scale environmental changes and pitch effects on the zenith angle position. To compute water dielectric constant and sea surface roughness, we included in the inverse model the actual sea salinity and temperature (measured by the thermosalinograph at 5 m depth) and wind speed (at 17 m height). The dielectric constant model we used was that of *Klein and Swift* [1977].

[40] According to bulk measurements, the sea had been warmer than the air for the entire experiment, implying unstable atmospheric conditions. The difference of air minus bulk sea temperature ranged from  $0.2^{\circ}\text{C}$  and  $-4.9^{\circ}\text{C}$ , with a mean value of  $-0.7^{\circ}\text{C}$ , while mean air and sea temperatures were  $27.8^{\circ}\text{C}$  and  $28.5^{\circ}\text{C}$ , respectively. Absolute wind speed ranged between 2.4 m/s and 12.7 m/s with a mean of 5.6 m/s, coming mainly from the northeast.

[41] For the same time interval, in Figure 10 we show the interface effect, which is the difference between the radiometric skin temperature (from MWSR and IRSR) and the in situ bulk temperature measured at 5 m depth. We did not use measurements from the drifting sea temperature sensor because we were not sure about the actual depth. In fact, especially when the ship was anchored, as in the days we are considering, such a

---

**Figure 7.** (opposite) Mean value (BIAS), standard deviation (STD: dashed-dotted) and root mean square (RMS: dotted) difference between radiometric estimations and in situ measurements for the entire sample (22 cases). (top) MWSR. (bottom) IRSR. The solid lines in the RMS and STD plots represent a priori estimates of temperature profile retrieval accuracy.

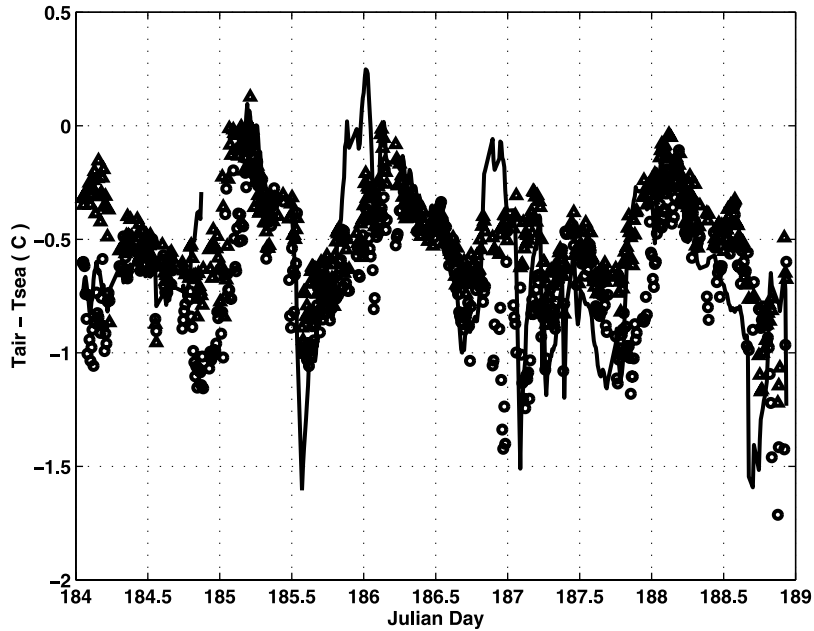


**Figure 9.** Five-day time series of air/sea temperature difference retrieved from downward looking MWSR and IRSR scans as well as bulk measurements. Estimates were obtained by averaging measured scans for 10 min. Julian day 184 corresponds to 1999/07/03; 189 to 1999/07/08 UTC. Triangles, MWSR; circles, IRSR; solid line, bulk.

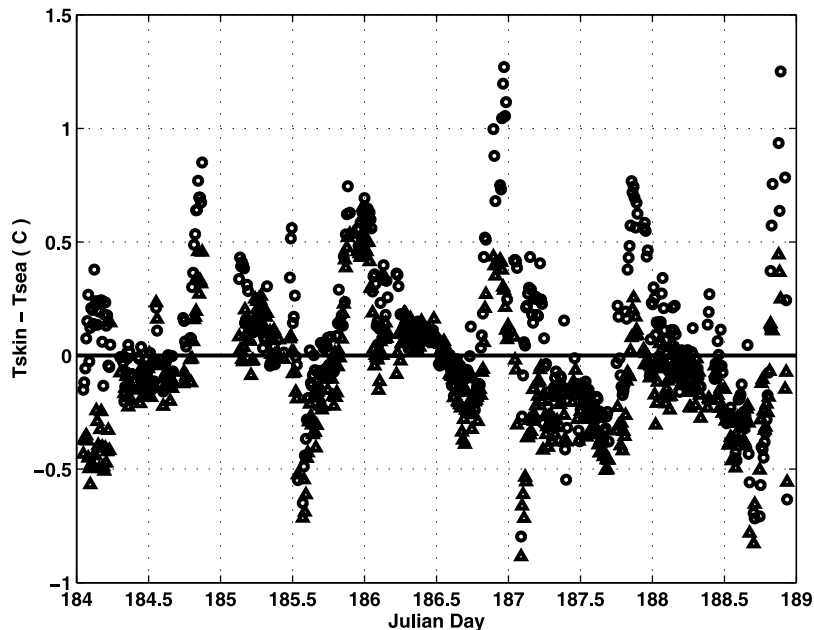


**Figure 10.** Five-day time series of interface effect for 10 min-averaged data. Julian day 184 corresponds to 1999/07/03 while 189 to 1999/07/08 UTC. Triangles, MWSR; circles, IRSR. Since Nauru Island is 12 hours ahead of UTC, local daytime is around midnight (0:00) UTC, whereas local nighttime is around noon (12:00) UTC. According to solar radiation, the time edge between day and night was set at 7 and 19 UTC; i.e., local daytime is between 19 and 7 UTC, local nighttime is between 7 and 19 UTC.

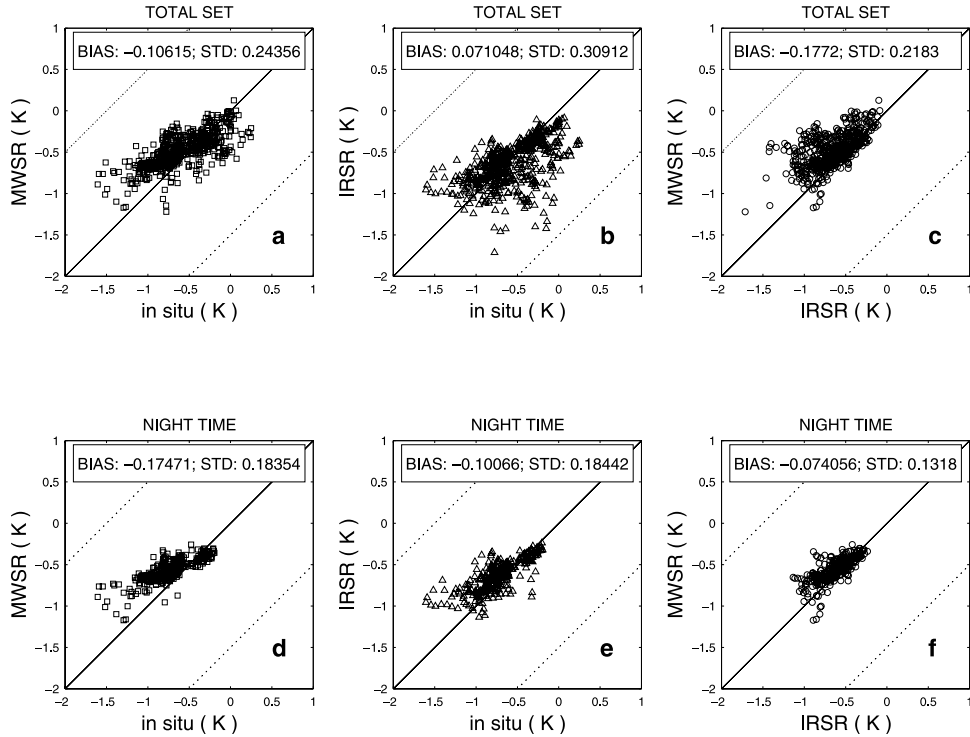


**Figure 11.** Scatterplots of air/sea temperature differences as retrieved from MWSR and IRSR downward looking scans and as measured by in situ sensors. Scatterplots are divided into MWSR-retrieved versus in situ measured (a and d), IRSR-retrieved versus in situ measured (b and e) and MWSR-retrieved versus IRSR-retrieved (c and f). For each of those comparisons we show the entire set of data (top: a, b, and c) and during local night hours (bottom: d, e, and f).

device might sink, leaving the actual depth unknown. Although there are some differences, the interface effect measured by MWSR and IRSR shows a similar behavior. The main departures happened during local daytime (around midnight UTC), remaining qualitatively within the values predicted by accuracy simulations. During local nighttime (around noon UTC) the agreement is impressive. It is promising to see that both the radiometers seem to follow the spikes related to very sharp and intense air temperature drops (at  $\sim 185.6$ , 187.1, 188.65 and 188.9 UTC Julian day). However, with the spatial resolution of these radiometers, and the temporal resolution we have chosen (10 min), we tend to smooth such sharp changes, and we do not expect to resolve them completely.

[42] In Figure 11 we present a series of scatterplots of air/sea temperature difference as retrieved from MWSR and IRSR downward looking scans and as measured by in situ sensors. Scatterplots are divided into MWSR-retrieved versus in situ measured (Figures 11a and 11d), IRSR-retrieved versus in situ measured (Figures 11b and 11e) and MWSR-retrieved versus IRSR-retrieved (Figures 11c and 11f). For each of those comparisons we

show the entire set of data (top: Figures 11a, 11b, and 11c) and during local night hours (bottom: Figures 11d, 11e, and 11f). According to the solar radiation, the time edge between day and night was set at 7 and 19 UTC; i.e., local daytime is between 19 and 7 UTC and local nighttime is between 7 and 19 UTC. For each scatterplot we report computed statistics (BIAS and STD) obtained after purging those data that fell outside of a predicted area of  $\pm 1.5$  K; this value corresponds to at least 4 times the computed STD. For convenience, BIAS, STD, RMS and correlation coefficients (COR) obtained from these samples are summarized in Table 2.

[43] Scatterplots and statistics both confirm that MWSR and IRSR retrievals are in good agreement during nighttime. Both of them appear to measure a sea skin colder than the bulk, and except for the sharp spikes, the difference ranges between 0.1 up to 0.5 K. These are qualitatively and quantitatively in agreement with the theory of cooling heat flux, which predicts a cool skin during nighttime [Schuessel *et al.*, 1990; Fairall *et al.*, 1996; Wick *et al.*, 1996]. Note that in the scatterplot between IRSR and MWSR measurements and in situ (Figures 11a, 11b, 11d, and 11e), they are not

**Table 2.** BIAS, STD, RMS, and COR for Air/Sea Temperature Difference Comparison Between Radiometric Estimates (MWSR and IRSR) and in Situ Measurements

	BIAS	STD	RMS	COR
	<i>Total</i>			
MWSR versus in situ	-0.106	0.243	0.265	0.719
IRSR versus in situ	0.071	0.309	0.317	0.515
MWSR versus IRSR	-0.177	0.218	0.281	0.601
	<i>Daytime</i>			
MWSR versus in situ	-0.029	0.277	0.279	0.564
IRSR versus in situ	0.261	0.308	0.404	0.570
MWSR versus IRSR	-0.291	0.237	0.376	0.696
	<i>Nighttime</i>			
MWSR versus in situ	-0.174	0.183	0.253	0.792
IRSR versus in situ	-0.100	0.184	0.210	0.751
MWSR versus IRSR	-0.074	0.131	0.151	0.728

equally distributed along the diagonal, but both show a change in slope. This change in slope shows that the air/sea temperature difference is much less with the skin rather than the 5-m bulk measurement and also has less dynamic range. Because of immediate physical contact, the ocean skin temperature is closely coupled to the overlying air temperature. Therefore, the air/sea temperature difference using the radiometric estimates tends to be smaller than that same difference measured by in situ sensors. This is especially pronounced in low wind speed conditions, when the mixing is diminished. The mean difference in the radiometric estimates is of the order of 0.07 K, while the dispersion is about 0.13 K, leading to a rms difference of about 0.15 K. During daytime the situation is much different, with a BIAS and a STD between MWSR and IRSR measurements twice as large as during nighttime. The strong solar radiation heats up the sea surface, which absorbs a large fraction of the downwelling radiation. This causes a “warm layer” at the top of the sea, which leads to a temperature difference between the skin and the bulk (5 m depth) ranging from 0 to 3 K, depending on wind speed and solar flux. This effect has a diurnal time scale and so can compensate the cool skin during daytime [Fairall *et al.*, 1996]. Moreover, the radiation absorption rate depends on skin depth and it might cause a difference between MWSR and IRSR measurements. Considering the total set, the IRSR mean measurement is warmer than the MWSR by about 0.18 K, while the STD is 0.22 K, for a RMS difference of 0.28 K. We note that, in contrast to theory of near surface temperature profile, the IRSR daytime measurements of skin temperature are warmer than those measured by the MWSR. We believe that this effect is an artifact of our IRSR calibrations, which relies on FTIR measurements as a zenith calibration point. The FTIR instrument was located on the deck of the ship,

whereas the IRSR was located on a boom over the water. Therefore, during the day, the air over the FTIR was often warmer than the air over the boom, and hence led to the observed bias. For example, we observed air temperature differences of as much as 5 K between two sensors that were placed at different locations on the ship.

## 6. Comments and Conclusions

[44] Some adjustments are suggested to improve the current system in future deployment. Although we believe that the overall calibration was as accurate as 0.2 K and that short time scale gain fluctuations are negligible for our averaging time interval (10 min), it would be useful to modify the present system to include at least one external calibration source. The brightness temperature of this source should be maintained at a value about 5 K lower than the ambient temperature, which would usually cover the dynamical range of temperatures expected in the measurement. The temperature control does not need very high precision, as long as the value is continuously measured and stored. In this case we could calibrate the radiometer’s gain every scan, using the target and horizontal view as two calibration sources. We could thus check on long term gain drift, as well as short-time-scale gain fluctuations, which would allow us to achieve the same precision while averaging for a shorter time interval (30/60 sec), resulting in an improved temporal and angular resolution.

[45] Another issue was the occurrence of foam on the sea surface. In the microwave region, foam emits as a blackbody, complicating the expected behavior of the MWSR scan and the concept of water skin layer itself. For this reason we limited our analysis to days for which the wind speed was lower than 8–9 m/s, which is believed to be the threshold for breaking waves in open ocean. Moreover, although the boom on which the system was mounted extended 5 m beyond the port side of the ship, it is possible that the motion of the ship itself could cause breaking waves and foam on the sides, which could enter the MWSR field of view. For this reason we chose to restrict our analysis further to those days in which the ship was mainly at rest. The experimental set up could be improved by locating the system, with the same boom-trolley configuration, on the ship’s bow, with the boom lying along the ship’s direction and the radiometers scanning across the ship’s direction. Thus the radiometers could scan over undisturbed and foam-free water even when the ship is moving, unless the wind speed exceeds the breaking waves threshold or the ship speed is high enough to generate forward propagating waves. Such a mounting technique, however, would place the radiometers in a position somewhat more susceptible to sea spray.

[46] Because of the increasing relevance of the final products obtainable by radiometric measurements, it is of great interest to propose new techniques, to study new calibration methods, and to quantify the accuracy achievable for the direct measurements and for the derived quantities. During Nauru99, NOAA/ETL introduced a new instrument, an infrared scanning radiometer, to complement an existing microwave scanning radiometer. Coupling natural radiation intensity measurements at infrared and microwave frequencies with appropriate inversion techniques provides independent robust estimation of simultaneous air temperature profile and air/sea temperature difference. The experimental set up enabled the radiometers to scan over undisturbed water, while maintaining easy and convenient access to the instruments. The gain of both radiometers was calibrated before the experiment with laboratory tests and comparison with simulation from radiosonde observations. A correction depending on internal temperature was applied to the MWSR gain, based on comparison with forward model predictions. For the IRSR we derived calibration coefficients using infrared spectroradiometer measurements during clear sky periods. We applied the same inversion techniques to measurements from each radiometer independently, using two different approaches for air temperature profile and air/sea temperature difference. For air temperature profile retrieval, we used a variation of linear statistical inversion based on empirical orthogonal functions, with an a priori data set prepared by processing almost 1500 ship RAOBs collected during TOGA COARE, with MODTRAN4 (for the IRSR) and Rosenkranz 98 (for the MWSR) forward models. Since air/sea temperature difference is a “well posed” problem, we used a physical inversion method, which accounts for air attenuation and emission and for effects induced by sea surface roughness.

[47] With such an instrument design, coupled with the appropriate inversion techniques, we achieved retrieval accuracy better than 0.3 K for air temperature profiles up to 500 m, and about 0.28 K for air/sea temperature differences, which becomes 0.15 K for nighttime measurements. Assuming that the instrumental random errors for the MWSR, the IRSR, and the radiosonde sensors are uncorrelated, we are able to say that the experiment achieved a RMS retrieval accuracy as low as 0.21 K for air temperature profiles up to 500 m and 0.20 for air/sea temperature differences, with the last decreasing to 0.11 K for nighttime measurements. These values validate the accuracy estimated by previous investigators [Trokhimovski et al., 1998; Westwater et al., 1998; Shaw et al., 2001], who considered a single scanning radiometer. These values also meet the accuracy required by marine boundary layer models to study the parameterization of atmosphere-ocean interactions [Schluessel et al., 1990; Fairall et al., 1996; Wick et al., 1996].

[48] To our knowledge this experiment was the first to compare two independent scanning radiometers operating at different spectral bands. Either or both instruments when providing high temporal measurements of both the surface temperature and the atmospheric temperature profile some 500 m above it, could add to the knowledge of the mutual interaction of the coupled ocean-atmosphere system. In addition, the different ocean skin penetration depths of the infrared and microwave instruments could provide information on near surface temperature gradient.

[49] We have demonstrated that scanning radiometry can provide accurate, continuous, simultaneous estimates of air temperature profile and air/sea temperature difference, and thus we believe that scanning radiometry represents a relatively simple, yet powerful tool to study the marine boundary layer environment.

[50] **Acknowledgments.** The work presented in this paper was sponsored by the Environmental Sciences Division of the Department of Energy as a part of their Atmospheric Radiation Measurement Program. The contributions of D. Cimini formed a portion of his Ph.D. thesis at the University of L’Aquila. The authors also thank Gary Wick, Sandra Castro, and Marian Klein for useful and insightful comments on the manuscript. We also thank Chris Fairall and Jeff Hare for providing in situ data.

## References

- Berk, A., L. S. Bernstein, G. P. Anderson, P. K. Acharya, D. C. Robertson, J. H. Chetwynd, and S. M. Adler-Golden, MODTRAN cloud and multiple scattering upgrades with application to AVIRIS, *Remote Sens. Environ.*, 65, 367–375, 1998.
- Bernstein, L. S., A. Berk, P. K. Acharya, D. C. Robertson, G. P. Anderson, J. H. Chetwynd, and L. M. Kimball, Very narrow band model calculations of atmospheric fluxes and cooling rates, *J. Atmos. Sci.*, 53(19), 2887–2904, 1996.
- Bolotnikova, G. A., S. I. Grechko, V. G. Irisov, A. V. Kuzmin, Y. G. Trokhimovski, and V. S. Etkin, Determination of the sea surface temperature from microwave radiometer measurements in the nadir, *Sov. J. Remote Sens.*, 9(4), 688–698, 1992.
- Clough, S. A., The water vapor continuum and its role in remote sensing, in *Optical Remote Sensing of the Atmosphere*, *Opt. Soc. of Am. Tech. Dig. Ser.*, vol. 2, pp. 76–78, Opt. Soc. of Am., Washington, D. C., 1995.
- Clough, S. A., M. J. Iacono, and J. L. Moncet, Line-by-line calculation of atmospheric fluxes and cooling rates: Application to water vapor, *J. Geophys. Res.*, 97(15), 15,761–15,785, 1992.
- Cox, C., and W. Munk, Measurements of the roughness of the sea surface from photographs of the sun’s glitter, *J. Opt. Soc. Am.*, 44(11), 838–850, 1954.
- Ewing, G., and E. D. McAlister, On the thermal boundary layer of the ocean, *Science*, 131, 1374–1376, 1960.

- Fairall, C. W., E. F. Bradley, J. S. Godfrey, G. A. Wick, J. B. Edson, and G. S. Young, Cool-skin and warm layer effects on sea surface temperature, *J. Geophys. Res.*, 101(C1), 1295–1308, 1996.
- Hadamard, J., *Le Probleme de Cauchy et les Equations aux Derives Partielles Lineares Hyberboliques*, Herman, Paris, 1932.
- Han, Y., J. A. Shaw, J. H. Churnside, P. D. Brown, and S. A. Clough, Infrared spectral radiance measurements in the tropical Pacific atmosphere, *J. Geophys. Res.*, 102(D4), 4353–4356, 1997.
- Hwang, P. A., and O. H. Shemdin, The dependence of sea surface slope on atmospheric stability and swell conditions, *J. Geophys. Res.*, 93(C11), 13,903–13,912, 1998.
- Klein, L. A., and C. T. Swift, An improved model for the dielectric constant of sea water at microwave frequencies, *IEEE Trans. Antennas Propag.*, AP25, 104–111, 1977.
- Leusky, V., V. G. Irisov, E. R. Westwater, L. S. Fedor, and B. Patten, Airborne measurements of the sea/air temperature differences by a scanning 5-mm wavelength radiometer, in *Proceedings of the International Geoscience and Remote Sensing Symposium/IGARSS '00*, pp. 260–262, 24–28 July, Honolulu, Hawaii, 2000.
- Liebe, H. J., and D. H. Layton, Millimeter wave properties of the Atmosphere: Laboratory studies and propagation modeling, *Rep. 87-24*, 74 pp., Natl. Telecommun. and Inf. Admin., Washington, D. C., 1987.
- McAlister, E. D., W. McLeish, and E. A. Gorduan, Airborne measurements of the total heat flux from the sea during BOMEX, *J. Geophys. Res.*, 76, 4172–4180, 1971.
- McKeown, W., F. Bretherton, H. L. Huang, W. L. Smith, and H. E. Revercomb, Sounding the skin of water: Sensing air-water interface temperature gradients with interferometry, *J. Atmos. Oceanic Technol.*, 12, 1313–1327, 1995.
- Mikhailova, D. V., and I. M. Fuks, Emissivity of a statistically rough surface including multiple reflection, *J. Commun. Technol. Electron.*, 38(11), 1993.
- Minnett, P. J., R. O. Knuteson, F. A. Best, B. J. Osborne, J. A. Hanafin, and O. B. Brown, The Marine-Atmospheric Emitted Radiance Interferometer (M-AERI), a high accuracy, sea-going infrared spectroradiometer, *J. Atmos. Oceanic Technol.*, 18, 994–1013, 2001.
- Nalli, N. R., W. L. Smith, and B. Huang, Quasi-specular model for calculating the reflection of atmospheric-emitted infrared radiation from rough water surface, *Appl. Opt.*, 40(9), 1343–1353, 2001.
- Pospelov, M. N., Surface wind speed retrieval using passive microwave polarimetry: The dependence on atmospheric stability, *IEEE Trans. Geosci. Remote Sens.*, 34(5), 1166–1171, 1996.
- Rosenkranz, P. W., Water vapor microwave continuum absorption: A comparison of measurements and models, *Radio Sci.*, 33(4), 919–928, 1998.
- Schluessel, P., W. J. Emery, H. Grassl, and T. Mammen, On the bulk-skin temperature difference and its impact on satellite remote sensing of sea surface temperature, *J. Geophys. Res.*, 95(C8), 13,341–13,356, 1990.
- Schroeder, J. A., and E. R. Westwater, Users' guide to WPL microwave radiative transfer software, *NOAA Tech. Memo, ERL-WPL 213*, 84 pp., 1991.
- Shaw, J. A., and J. H. Churnside, Scanning-laser glint measurements of sea-surface slope statistics, *Appl. Opt.*, 36(18), 4202–4213, 1997.
- Shaw, J. A., D. Cimini, E. R. Westwater, Y. Han, H. M. Zorn, and J. H. Churnside, A scanning infrared radiometer for measuring air/sea temperature difference, *Appl. Opt.*, 40(27), 4807–4815, 2001.
- Smirnov, A. V., Polarimetric radar imagery of the ocean at low grazing angles under atmospheric condition of variable stability, in *Proceedings of the International Geoscience and Remote Sensing Symposium/IGARSS'94*, pp. 805–807, Pasadena, Calif., 1994.
- Smith, S. D., Coefficients for sea surface wind stress, heat flux, and wind profiles as a function of wind speed and temperature, *J. Geophys. Res.*, 93, 15,467–15,472, 1988.
- Strang, G., *Linear Algebra and its Applications*, Academic, San Diego, Calif., 1980.
- Trokhimovski, Y. G., E. R. Westwater, Y. Han, and V. Leuski, Air and sea surface temperature measurements using a 60-GHz microwave rotating radiometer, *IEEE Trans. Geosci. Remote Sens.*, 36(1), 3–15, 1998.
- Vesecky, J. F., R. G. Onstott, N. Y. Wang, E. Lettvin, J. Slawski, and R. A. Shuchman, Water surface temperature estimates using active and passive microwave remote sensing: Preliminary results from an outdoor wind-wave tank, in *Proceedings of the International Geoscience and Remote Sensing Symposium/IGARSS'94*, pp. 1021–1023, Pasadena, Calif., 1994.
- Webster, P. J., and R. Lukas, TOGA COARE: The Coupled Ocean Atmosphere Response Experiment, *Bull. Am. Meteorol. Soc.*, 73, 1377–1416, 1992.
- Westwater, E. R., Ground based microwave remote sensing of meteorological variables, in *Atmospheric Remote Sensing by Microwave Radiometry*, edited by M. Janssen, pp. 145–213, John Wiley, New York, 1993.
- Westwater, E. R., Y. Han, V. G. Irisov, V. Y. Leusky, Y. G. Trokhimovski, C. W. Fairall, and A. Jessup, Sea-air and boundary layer temperatures measured by a scanning 5-mm-wavelength radiometer: Recent results, *Radio Sci.*, 33(2), 291–302, 1998.
- Westwater, E. R., Y. Han, V. G. Irisov, V. Leusky, E. N. Kadyrov, and S. A. Viazankin, Remote sensing of boundary layer temperature profiles by a scanning 5-mm microwave radiometer and RASS: Comparison experiment, *J. Atmos. Oceanic Technol.*, 16(7), 805–818, 1999.
- Westwater, E. R., Y. Han, and F. Solheim, Resolution and accuracy of a multi-frequency scanning radiometer for temperature profiling, in *Microwave Radiometry and Remote Sensing of the Earth's Surface and Atmosphere*, edited by P. Pampaloni and S. Paloscia, pp. 129–135, VSP Press, 2000.
- Wick, G. A., W. J. Emery, L. H. Kantha, and P. Schluessel, The behaviour of the bulk-skin sea surface temperature differ-

- ence under varying speed and heat flux, *J. Phys. Oceanogr.*, 26, 1969–1987, 1996.
- Wu, X., and W. L. Smith, Emissivity of rough sea surface for 8–13 microns: Modeling and verification, *Appl. Opt.*, 36(12), 2609–2619, 1997.
- 
- J. H. Churnside, V. Irisov, V. Leuski, and E. R. Westwater, Environmental Technology Laboratory, 325 Broadway MS R/E/ET1, Boulder, CO 80305, USA. (Vladimir.Irisov@noaa.gov; Vladimir.Leuskiy@noaa.gov; Ed.R.Westwater@noaa.gov)
- D. Cimini, CETEMPS, University of L'Aquila, Via Vetoio 1, Coppito, L'Aquila I-67010, Italy. (nico.cimini@aquila.infn.it)
- Y. Han, NOAA NESDIS, WWB Room 810, 5200 Auth Road, Camp Springs, MD 20746, USA. (Yong.Han@noaa.gov)
- J. Shaw, Electrical and Computer Engineering Department, 610 Cobleigh Hall, Montana State University, Bozeman, MT 59717, USA. (jshaw@ece.montana.edu)